DOI: 10.4408/IJEGE.2020-01.S-15

# PHYSICAL MODEL TESTS ON SPAR BUOY FOR OFFSHORE FLOATING WIND ENERGY CONVERSION

Giuseppe Roberto TOMASICCHIO(*), Diego VICINANZA(**), Marco BELLOLI(***), Claudio LUGNI(****), John-Paul LATHAM(*****), Jose Gregorio IGLESIAS RODRIGUEZ(******), Bjarne JENSEN(*******), Axelle VIRE(********), Jaak MONBALIU(*********), Federico TARUFFI(***), Luca PUSTINA(**********), Elisa LEONE(*), Sara RUSSO(**), Antonio FRANCONE(*), Alessandro FONTANELLA(***), Simone DI CARLO(***), Sara MUGGIASCA(***), Griet DECORTE(*********), Irene RIVERA-ARREBA(********), Vincenzo FERRANTE(**), Tommaso BATTISTELLA(***********), Raul GUANCHE GARCIA(***********), Abel MARTÍNEZ DÍAZ(******), Björn ELSÄSSER(*******), Lluis VIA-ESTREM(*****), Jiansheng XIANG(*****), Morten Thøtt ANDERSEN(************), Jens Peter KOFOED(************), Morten Bech KRAMER(************), Elena MUSCI(*************), Letizia LUSITO(*)

(*)University of Salento, Via per Monteroni, Lecce, Italy .

(**)University of Campania, Viale Abramo Lincoln 5, Caserta, Italy.

(***)Polytechnic University of Milan, Department of Mechanical Engineering, via La Masa 1, Milano, Italy.

(****)CNR (National Research Council), Italy.

(*****)Imperial College London, Department of Civil and Environmental Engineering, South Kensington Campus, London, England.

(******)University College Cork, Ringaskiddy, Cork, Ireland.

(*******)DHI Water & Environment, Hørsholm, Denmark.

(********)Delft University of Technology, Mekelweg 5, Delft, Netherlands.

(*********)Catholic University of Leuven, Department of Civil Engineering, Kasteelpark Arenberg 40, Leuven, Belgium.

(**********)Roma Tre University, Via della vasca navale, Roma, Italy.

(***********)University of Cantabria, Calle Isabel Torres 15, Parque Científico y Tecnológico de Cantabria, Santander, Spain.

(************)Aalborg University, Dept. of Civil Engineering, Thomans Manns Vej 23, Aalborg, Denmark.

(*************)AGENIA S.r.l., Piazza Galileo 6, Bologna, Italy .

Corresponding author: roberto.tomasicchio@unisalento.it

## EXTENDED ABSTRACT

La domanda globale di energia eolica sta aumentando rapidamente e sta acquisendo sempre più importanza come risorsa energetica, dato l'interesse crescente per le energie rinnovabili. Le risorse eoliche offshore hanno attirato un'attenzione significativa e, rispetto alle risorse eoliche terrestri, sembrano essere più promettenti per lo sviluppo. I venti marini sono generalmente più forti e più affidabili e grazie agli enormi miglioramenti della tecnologia, il mare è diventato un hot spot per nuovi design e metodi di installazione per le turbine eoliche. C'è molto interesse in questo campo, poiché si ritiene che svolga un ruolo importante nel futuro dell'eolico offshore.

Vari carichi dinamici vengono trasmessi dalla torre della turbina eolica alla sua piattaforma: carico del vento, carico delle onde del mare, carico dinamico dovuto al rotore, effetti di schermatura del vento della pala sulla torre che crea un carico ciclico. Per una turbina eolica offshore che opera sulla superficie del mare in continua evoluzione, è quindi fondamentale studiare il comportamento dinamico a cui è soggetta la struttura e in che modo la complessa interazione dei carichi delle onde e del vento influisca sul sistema.

Un robusto processo di progettazione deve garantire che la frequenza naturale dell'intero sistema non si avvicini alle frequenze dei carichi ambientali imposti. In caso contrario, si potrebbe amplificare la risposta dinamica della struttura, portando a maggiori deflessioni della torre che possono compromettere le prestazioni della turbina eolica. Le turbine eoliche galleggianti sono supportate da strutture galleggianti e, quindi, hanno 6 gradi di libertà, che possono essere eccitate da carichi di onde, vento e correnti oceaniche. L'intero sistema è ormeggiato e stabilizzato mediante un sistema di molle e contrappesi. Sono strutture relativamente grandi che variano tra 5000 e 10.000 tonnellate per un'unità da 2 a 5 MW. Le turbine eoliche galleggianti sono soggette a carichi di vento e anche la struttura di supporto è soggetta a carichi idrodinamici, innescando un comportamento non lineare complesso dovuto alla combinazione di questi carichi. I carichi del vento che agiscono sulle pale della turbina eolica vengono trasmessi alla piattaforma galleggiante attraverso i componenti rotore-

navicella e le torri; allo stesso tempo, anche la tensione di ormeggio ricevuta dal sistema di ormeggio viene trasmessa alla piattaforma galleggiante. Questi influenzano la risposta dinamica della piattaforma mobile. D'altra parte, il movimento della piattaforma galleggiante a sua volta provoca un movimento relativo tra la piattaforma e le pale della turbina eolica, influenzando le forze aerodinamiche sulle pale. Le reazioni tra le varie componenti della struttura sono complesse e accoppiate, rendendo la risposta dinamica del sistema FOWT difficile da prevedere e piena di sfide. Il sistema di accoppiamento pale-torre-piattaforma non è lineare, elemento di novità rispetto alle strutture tradizionali.

Sono stati condotti esperimenti di alta qualità per esaminare la risposta dinamica della turbina eolica offshore. Sono stati condotti esperimenti utilizzando le strutture del DHI (Danish Hydraulic Institute) nell'ambito dell'iniziativa EU-Hydralab + Integrated Infrastructure Initiative utilizzando una turbina eolica di riferimento NREL 5MW in scala 1:40 (RWT) posta su piattaforma galleggiante OC3-Hywind, un concetto sviluppato da Statoil della Norvegia costituito da un unico cilindro verticale di grande diametro. Sono stati simulati diversi carichi dinamici che agiscono sulla turbina eolica galleggiante offshore, derivanti da una combinazione di attacchi di onde regolari e irregolari a cresta lunga ortogonali (0°) e obliqui (20°) alla struttura e diversi carichi del vento. Gli effetti delle alte frequenze non sono stati considerati in questo documento e la ricerca considera la torre della turbina eolica come un corpo rigido, quindi solo i sei gradi di libertà della piattaforma sono considerati per calcolare la risposta a bassa frequenza della piattaforma. Sono state implementate tecniche di elaborazione del segnale sui dati acquisiti al fine di valutare le principali proprietà dinamiche della struttura offshore. In primo luogo, è stata studiata la risposta strutturale dopo l'applicazione di un impulso, consentendo di ottenere la frequenza naturale di ciascun grado di libertà a cui è soggetta la struttura offshore e di identificare i rapporti di smorzamento modale. Successivamente, sono stati presentati i risultati relativi alle onde regolari, con incidenza ortogonale alla struttura; i test selezionati hanno considerato un'onda regolare con lo stesso periodo al fine di analizzare l'influenza dell'altezza dell'onda senza carico del vento e con un carico del vento che consente al rotore della turbina eolica di raggiungere la condizione nominale. Sono state effettuate analisi di spostamenti, rotazioni, accelerazioni, risposta delle forze della struttura galleggiante e delle linee di ormeggio. I risultati mostrano che la maggior parte della risposta dinamica longitudinale si verifica alla frequenza dell'onda con un contributo minore, ma non trascurabile, alle frequenze del corpo rigido, in contrasto con la risposta dinamica laterale in cui le frequenze del corpo rigido sono predominanti.

## ABSTRACT

The present paper describes the experiences gained from the design methodology and operation of a 3D physical model experiment aimed to investigate the dynamic behaviour of a spar buoy floating offshore wind turbine. The physical model consists in a Froude-scaled NREL 5MW reference wind turbine (RWT) supported on the OC3-Hywind floating platform. Experimental tests have been performed at Danish Hydraulic Institute (DHI) offshore wave basin within the European Union-Hydralab+ Initiative, in April 2019. The floating wind turbine model has been subjected to a combination of regular and irregular wave attacks and different wind loads. Measurements of displacements, rotations, accelerations, forces response of the floating model and at the mooring lines have been carried out. First, free decay tests have been analysed to obtain the natural frequency and the modal damping ratios of each degree of freedom governing the offshore. Then, the results concerning regular waves, with orthogonal incidence to the structure, are presented. The results show that most of longitudinal dynamic response occurs at the wave frequency and most of lateral dynamic response occurs at rigid-body frequencies.

***Keywords****: offshore structures, floating wind turbine, hydrodynamic behavior, spar buoy.*

## INTRODUCTION

In 2018 wind energy met about 14% of Europe's total energy demand, of which 10% can be attributed to the offshore wind industry, assuring Europe's leading role in offshore wind energy (Windeurope, 2019). The share of offshore wind is poised to rise significantly in the coming years thanks to its advantages relative to its onshore counterpart: no impact on inhabited land and, therefore, no urban planning constraints; greater social acceptability; and a larger, less variable resource. For these reasons, offshore wind is rapidly becoming financially viable (Bilgili *et alii*, 2011; Riefolo *et alii*, 2016).

The vast majority of the development of offshore wind energy so far has involved substructures fixed to the seabed – monopiles, jacket frames, gravity-based foundations, etc. These seabed-fixed substructures are limited to water depths of up to 50 m. For this reason, offshore wind has developed in shallow areas, primarily in the North Sea. There remain many untapped marine regions close to the coast and with a significant resource, where seabed-fixed offshore wind turbines are not an option because of the large water depths: the Californian, Portuguese and Norwegian offshore regions are cases in point (Breton & Moe, 2009), as is most of the Mediterranean.

Floating offshore wind turbines (FOWTs) are the solution to harvest this resource. Three main types of floating substructures are being considered: (1) the spar-buoy, stable thanks to the righting moment provided by ballast at the bottom of the spar; (2) the semi-submersible platform, which draws its stability from its large water-plane area; (3) and the tension-leg platform, stabilized by taut cables pre-tensioned by buoyancy. These concepts have been scaled down from their respective counterparts commonly used in the oil and gas industry.

The aero-elastic effects, together with the slenderness of the structures and the smaller submerged volumes, which make drag predominant, are clear differences relative to previously built offshore structures (Roald *et alii*, 2013). Therefore, new research is necessary, including laboratory testing, to improve the current understanding not only of these specific innovative structures but also the complex behaviour of floating bodies. In this path, several models have been developed. Stockstill *et alii* (2009) used a dynamic method to calculate the acceleration exerted on the floating body. Petaccia *et alii* (2018) proposed a 2D method based on the one-way coupling of the Eulerian solution of the SWE and the Lagrangian Discrete Element (DE) dynamic description of the body transport.

A first objective of the paper is to provide reliable, high-quality data allowing improvements to numerical models dealing with the location of the rigid body in the grid domain and the assignment of the hydraulic parameters where the forces are calculated.

During Phase IV of OC3, a reference model for the floating offshore wind turbine of the spar-buoy type with the NREL 5MW wind turbine mounted on top has been developed based on the currently installed Hywind spar-buoys along the Scottish East Coast. The goal of this model was to enable code comparison in order to better appraise the current array of offshore wind turbine codes and to arrive at conclusions concerning future design practices with these codes (Jonkman, 2010; Jonkman *et alii*, 2010).

In addition, in 2012, Goupee et al. conducted wave basin tests for three floating offshore wind turbine concepts, one of them being the OC3 Hywind spar (Goupe *et alii*, 2014). However, although the simultaneously working wind and wave generator correctly modelled wind and waves, wind-wave misalignment was not studied. In 2014, as part of Hydralab IV, a wide array of directional and unidirectional wave cases were run on the OC3 Hywind spar-buoy in the Ocean Basin at DHI, Denmark. At the time no wind generator was available, and therefore an approximate system was used to model the wind (Tomasicchio *et alii*, 2018).

This paper presents the laboratory tests carried out at DHI in 2019 within Hydralab+ with the aim of addressing the above-mentioned knowledge and data gaps. The specific objectives of the tests were to correctly model the combined unidirectional and directional wave and wind loads in the presence of a wind generator (novelty compared to Hydralab IV), and to create a

reliable and accurate database for calibration and validation of numerical models. Additionally, the coupling between a pitch-controlled rotor and the hydrodynamics of the FOWT system (regarded as a rigid body) was investigated.

This article is structured as follows. First, the design of the model, its aerodynamics and hydrodynamics, are discussed. Second, the experimental campaign is presented. Third, a first analysis of the data collected during the tests is conducted, and the results presented. Finally, conclusions are drawn and further work from the users is introduced.

In addition, in 2012, Goupee et al. conducted wave basin tests for three floating offshore wind turbine concepts, one of them being the OC3 Hywind spar (Goupe *et alii*, 2014). However, although the simultaneously working wind and wave generator correctly modelled wind and waves, wind-wave misalignment was not studied. In 2014, as part of Hydralab IV, a wide array of directional and unidirectional wave cases were run on the OC3 Hywind spar-buoy in the Ocean Basin at DHI, Denmark. At the time no wind generator was available, and therefore an approximate system was used to model the wind (Tomasicchio *et alii*, 2018).

## DESIGN OF THE MODEL

*Aerodynamics*

The Hydralab+ wind turbine model is defined as a 1:40 model of the reference NREL 5MW, scaled according to Froude similarity rule, whose geometric and dynamic characteristics are listed in Table 1. The rotor is designed upscaling the PoliMi WTM, a 1:75 wind turbine model of the DTU 10MW RWT designed and currently utilized for wind tunnel tests on FOWT. The aerodynamic design procedure had to match the reference thrust and the reference torque.

The Hydralab+ rotor is designed as a geometrical upscale of the PoliMi WTM and the entire blade is designed using the SD7032 airfoil shown in Figure 1; only in the area near the blade root the blade section shape is interpolated with the circular section thus allowing a smooth transition to the circular section blade root. The selected airfoil differs from the ones applied for the NREL 5MW and the DTU 10MW in order to have better performances at the lower Reynolds numbers that characterize the airfoil aerodynamics for the wind tunnel tests.

The wind turbine model is equipped with a control and monitoring system and with actuators and sensors in order to ensure autonomous and continuous operation and to reproduce the reference full-scale turbine dynamics during experiments. The mechatronic of the wind turbine model is characterized by four actuators, a main shaft motor used to control the rotor angular speed and three dedicated motors allow to control in real-time the individual pitch angle of each blade. The turbine is also equipped with an encoder sensor measuring the generator

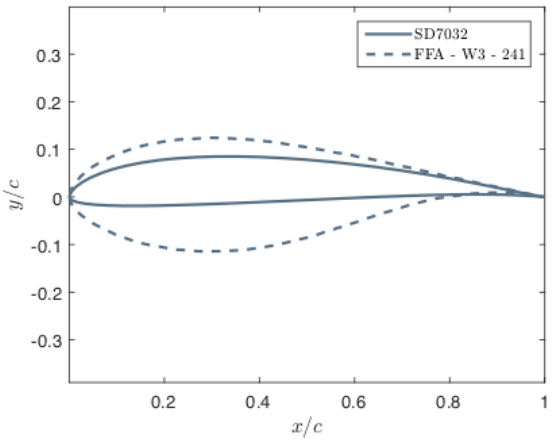


*Fig.1 - SD7032 low-thickness profile in comparison with the FFA profile used in the full scale turbine.*

speed used as controller feedback. An embedded system is capable to control the actuators and acquire data from sensors simultaneously.

The control system is designed starting from the NREL 5MW, and the parameters are obtained applying the same scaling rules. The wind turbine controller is based on the standard variable-speed variable-pitch control strategy used by modern wind turbines to regulate power production and rotor speed through the machine operating range. Some modifications

| | ***Full-scale*** | ***Model scale*** | ***Scale factor*** |
|---|---|---|---|
| ***Rotor orientation*** | ***Clockwise rotation - Upwind*** | | **-** |
| ***Control*** | ***Variable speed - Collective Pitch*** | | **-** |
| Number of blades | 3 | 3 | - |
| Rotor Diameter [m] | 126 | 3x15 | $\lambda$ |
| Hub Diameter [m] | 3 | 0.075 | $\lambda$ |
| Hub Height [m] | 90 | 2.25 | $\lambda$ |
| Rated wind speed [m/s] | 11.4 | 1.8 | $\lambda^{1/2}$ |
| Rotor speed (rated) [rpm] | 12.1 | 76.5 | $\lambda^{-1/2}$ |
| Ideal power [W] | $5x10^6$ | 12.35 | $\lambda^{7/2}$ |
| Rotor Mass [kg] | 110000 | 1.72 | $\lambda^3$ |
| Nacelle Mass [kg] | 240000 | 3.75 | $\lambda^3$ |

*Tab.1 - Downscaled properties of NREL 5MW wind turbine with model scale ratio (1/λ) = 1:40.*

were introduced with respect to the original controller to make more effective the implementation on the scale model. The control strategy adopted is variable-speed variable-pitch. In this scheme, the turbine is programmed to operate at variable-speed and fixed-pitch below rated wind speed, to optimize the power extraction efficiency, and at variable pitch above rated wind speed, to regulate rotor speed and power. The control system is characterized by 3 different regions of operation: Region 1, for wind speed until cut-in, it's used for the start-up of the wind turbine; Region 2 represent the partial-load operation and extends from cut-it to rated wind speed: in this region the blade pitch it's set fixed at its minimum and the turbine is regulated at variable speed through the torque controller; Region 3 extends from rated wind speed to the cut-off and the turbine works at full-load: in this region the generator torque is set at the rated value and the turbine operation is regulated by the blade pitch-to-feather PI controller.

*Hydrodynamic*

In order to adequately model the wave-structure interaction during the experiments, a 1/40 Froude scaled model OC3-Hywind spar buoy by Jonkman (2010) was adopted. Tomasicchio *et alii* (2018) have used this very same layout in the previous experiments undertaken as part of the Hydralab IV call (Tomasicchio *et alii*, 2012; Tomasicchio *et alii*, 2016). As can be seen in Figure 2, the spar buoy is in fact of very simple geometry; it consists of a hollow cylinder with a taper on top allowing for a smooth transition between the large immersed diameter needed for stability and the small diameter at the wind turbine-spar buoy interface. It also reduces the hydrodynamic loads at the water surface. No VIV suppressing devices were added, enabling us to take the vortex shedding effects along as well.

| | *Full-scale* | *Model scale* | *Scale factor* |
|---|---|---|---|
| *Platform diameter below taper [m]* | 9.4 | 0.23 | $\lambda$ |
| *Depth to the platform base below SWL [m]* | 130 | 3.25 | $\lambda$ |
| *Platform diameter above taper [m]* | 6.5 | 0.16 | $\lambda$ |
| *Depth to top of taper below SWL [m]* | 4 | 0.10 | $\lambda$ |
| *Depth to bottom of taper below SWL [m]* | 12 | 0.30 | $\lambda$ |
| *CM location below SWL [m]* | 89.91 | 2.25 | $\lambda$ |
| *Mass, including ballast [kg]* | 7466330 | 116.66 | $\lambda^3$ |
| *Roll inertia about CM [kg·m²]* | 4229230000 | 41.30 | $\lambda^5$ |
| *Pitch inertia about CM [kg·m²]* | 4229230000 | 41.30 | $\lambda^5$ |
| *Yaw inertia about center-line [kg·m2]* | 164230000 | 1.60 | $\lambda^5$ |

*Tab.2 - Downscaled properties of OC3-Hywind spar-buoy ($\lambda$ = 40).*

*Fig.2 - Downscaled spar-buoy model.*

To reach the correct draft and full system overall properties, i.e. the mass and center of gravity, the bottom of the cylinder has been partially filled by an assortment of small lead grains of several diameters. The downscaled properties of the spar buoy are listed in Table 2. For further details concerning the OC3-Hywind model, the reader is kindly referred to the work of Jonkman (Jonkman, 2010).

For the mooring system, the original crowfoot layout of catenary lines of the OC3-Hywind spar-buoy, was downscaled (Riefolo *et alii*, 2018). However, due to the limited available water depth at DHI's Ocean Basin, the original catenary lines from the OC3-Hywind project, had to be simplified after scaling down. As a result, each line was reduced to a series of seven springs connected to a mass (a concrete block) placed on the basin floor. Each spring configuration was designed in order to closely mimic the originally downscaled surge and sway behavior.

## EXPERIMENTAL CAMPAIGN

*Experimental layout*

The deep-water basin at DHI is 20 m long, 30 m wide and 3 m deep, with a 3 m x 3m and 6 m deep pit at the mid of the basin. Its wave maker is equipped with 60 individually controlled flaps, which are able to generate regular and irregular unidirectional and directional wave fields. To minimize reflection, a 6.5 m long sloping wave absorber is located opposite the wave maker.

The free surface elevation is captured by a row of three wave gauges at 1.5 m before the spar-buoy and a row of six wave gauges placed at 1 m behind the spar-buoy. Both sets of wave gauges are placed perpendicular to the wave direction. In addition, two more wave gauges are located at the back of the spar-buoy to allow for an array reflection analysis to obtain the incident and reflected waves (Mansard *et alii*, 1980).

These wave gauges are placed parallel with respect to the wave propagation. The far-field layout of basin and the wave gauge locations in the near-field area close to the FOWT are shown in Figure 3 together with the mooring system.

Wave elevation was sampled at 100 Hz for regular and irregular waves. The duration for regular wave cases is about 3 minutes and 20-30 minutes for the irregular wave cases. Furthermore, in case of large amplitude long waves, typically leading to Keulegan-Carpenter numbers larger than 7, vortex-shedding may occur in the small portion of the spar buoy just below the water level (Sumer & Mutlu, 2006).

In order to detect such vortex shedding effects, two Vectrino Acoustic Doppler Velocimeters were located close to each other at the back of the spar buoy. They were placed at an angle of 20 degrees with respect to the wave propagation. To evaluate the vertical distribution of the dynamic pressures, three pressure transducers are located on the spar-buoy in the splash region. The wave impact forces are then obtained by spatially integrating these pressure measurements.

A Qualisys Tracking System was used to track the six-degrees-of-freedom motion of the FOWT. In addition, the model is equipped with four accelerometers. Two inertial frames measuring the translational and angular accelerations along three axes were used; one located at the top of the spar buoy and another one at the nacelle. Two uniaxial accelerometers were placed on the tower to capture the acceleration along the global x- and y-axis. A load cell was placed at each mooring line connection to observe the tension force produced by the spar-buoy motion. An encoder placed in the wind turbine rotor allows measuring the angular velocity of the generator and, in addition, enables to track the reference for the blades' pitch. All observed data were synchronized by the DHI Wave Synthesizer.

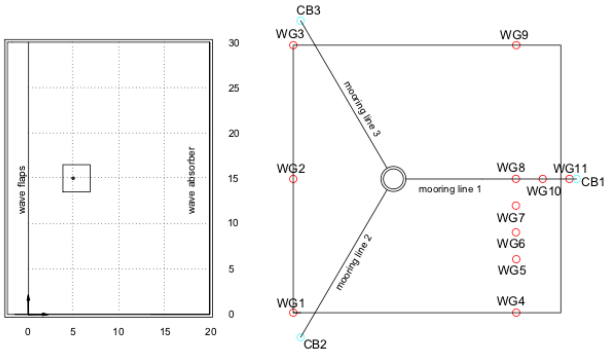


*Fig.3 - Wave basin layout (left) and wave gauge locations in the near-field area (right).*

*Load Analysis overview*

All the tests have been performed using different conditions of wave and wind. For what concern wave conditions, the assigned parameters characterizing a sea state, are wave height, wave period and wave direction, which are orthogonal (0°) and yawed (20°) to the structure; a distinction between regular and irregular waves must be done.

In Table 3 the characteristics of the generated waves are given, where $H$ and $T$ are the regular wave height and wave period, respectively, and $H_s$ and $T_p$ are the significant wave height and peak wave period, respectively. For the regular waves, each wave height has been coupled with each period, for both wave directions. For the irregular waves, each wave height has been characterized by its wave period, only wave direction changed.

Wind conditions are characterized by "no wind condition" and "rated condition" represented by value of wind speed of 1.85 m/s. In addition, some tests have been performed at

| *Wind speed* | *Waves* | *Prototype scale* | | | *Model scale* | | |
|---|---|---|---|---|---|---|---|
| | | *H or Hs [m]* | *T or Tp [s]* | *Dir [deg]* | *H or Hs [m]* | *T or Tp [s]* | *Dir [deg]* |
| *0 m/s (no wind) 1.85 m/s (rated)* | *Regular* | 2.0<br>5.2<br>10.0 | 5.1<br>7.0<br>8.9<br>10.1<br>12.0<br>13.9 | 0<br>20 | 0.05<br>0.13<br>0.25 | 0.8<br>1.1<br>1.4<br>1.6<br>1.9<br>2.2 | 0<br>20 |
| | *Irregular* | 2.4<br>3.2<br>4<br>6<br>8 | 7.1<br>9.7<br>7.3<br>9.1<br>10.7 | 0<br>20 | 0.06<br>0.08<br>0.10<br>0.15<br>0.20 | 1.12<br>1.53<br>1.15<br>1.44<br>1.69 | 0<br>20 |

*Tab. 3 - Physical model test program.*

| | Surge | | Sway | | Heave | | Pitch | | Roll | | Yaw | |
|---|---|---|---|---|---|---|---|---|---|---|---|---|
| ***Nominal wind [m/s]*** | 0 | 1.85 | 0 | 1.85 | 0 | 1.85 | 0 | 1.85 | 0 | 1.85 | 0 | 1.85 |
| ***f [Hz]*** | 0.09 | 0.09 | 0.07 | / | 0.22 | 0.22 | 0.20 | 0.18 | 0.18 | 0.17 | 0.39 | 0.30 |
| ***T (model scale) [s]*** | 11.11 | 11.11 | 14.28 | / | 4.55 | 4.55 | 5.00 | 5.55 | 5.55 | 5.88 | 2.56 | 3.33 |
| ***T (prototype scale) [s]*** | 70.26 | 70.26 | 90.31 | / | 28.77 | 28.77 | 31.62 | 35.10 | 35.10 | 37.18 | 16.19 | 21.06 |
| ***Bandpower [%]*** | 98.41 | 94.06 | 99.58 | / | 99.93 | 99.54 | 99.93 | 64.83 | 99.37 | 99.09 | 99.26 | 60.90 |
| ***Damping Coeff. a*** | 0.04 | 0.04 | 0.08 | / | 0.08 | 0.12 | 1.62 | 0.40 | 2.48 | 0.81 | 4.60 | 0.48 |
| ***Damping Coeff. b*** | -0.02 | -0.02 | -0.01 | / | -0.07 | -0.08 | -0.07 | -0.09 | -0.02 | -0.02 | -0.14 | -0,00 |

*Tab. 4 - Frequencies, natural periods, band power and damping coefficients of surge, sway, heave, roll, pitch and yaw: no wind conditions and above rated conditions*

different nominal wind speed values: 1.25 m/s, 1.45 m/s, 1.65 m/s, 1.95 m/s.

## EXPERIMENTAL CAMPAIGN

*Free decay tests*

Free decay tests have been carried out to evaluate the natural frequencies and periods, band power and damping coefficients of each DoF which characterize the exponentially decaying sinusoid equation. The mechanical energy of the system diminishes in time and the damping is represented by an exponentially decaying sinusoid characterized by coefficients *a* and *b*:

$$x = a \cdot e^{-bt} \tag{1}$$

The measured model-scale rigid body oscillation frequencies are shown in Table 4 together with natural periods, bandpower and damping coefficients of each DoF. Frequencies of order of ($10^{-2}$) in surge and sway and order of ($10^{-1}$) in pitch and roll have been found.

The damping ratio was calculated using the logarithmic decrement method, as a function of two response amplitudes $X_j$ and $X_{j+1}$, according to the following expression:

$$\xi = \frac{\delta}{\sqrt{4\pi^2 + \delta^2}} \tag{2}$$

Where $\delta = 1/j \ \ lnX_1/X_{j+1}$, $j$ being the number of the cycles taken into account (Karimira, 2014). To quantify the non-linear nature of damping, the damping ratios were calculated considering the average value of different number of cycles, as shown in Figure 4. In this case, the strong nonlinearity of damping in the first cycle could affect the average damping of the first five cycles.

Then, the damping ratios stabilize and become almost constant. In particular, values of 14.7%, 11.1%, 4.3%, 3.4%, 6.0%, 3.3% and 8.5% were found for surge, sway, heave, pitch, roll and yaw respectively when the first 7 cycles of oscillation were considered. The sway tests in above rated conditions were not conducted due to technical reasons.

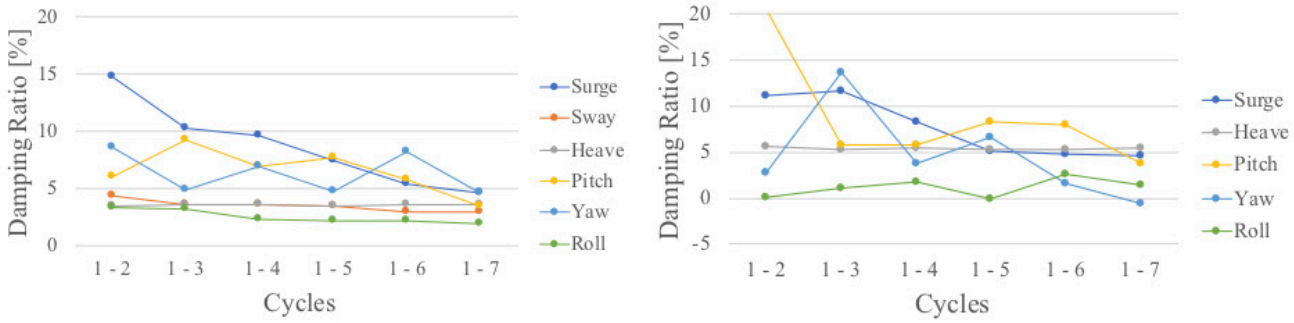


*Fig.4 - Damping ratio from free decay tests, obtained from the average logarithmic decrement considering the peaks $X_1$ and $X_{j+1}$: no wind conditions (left) and above condition (right).*

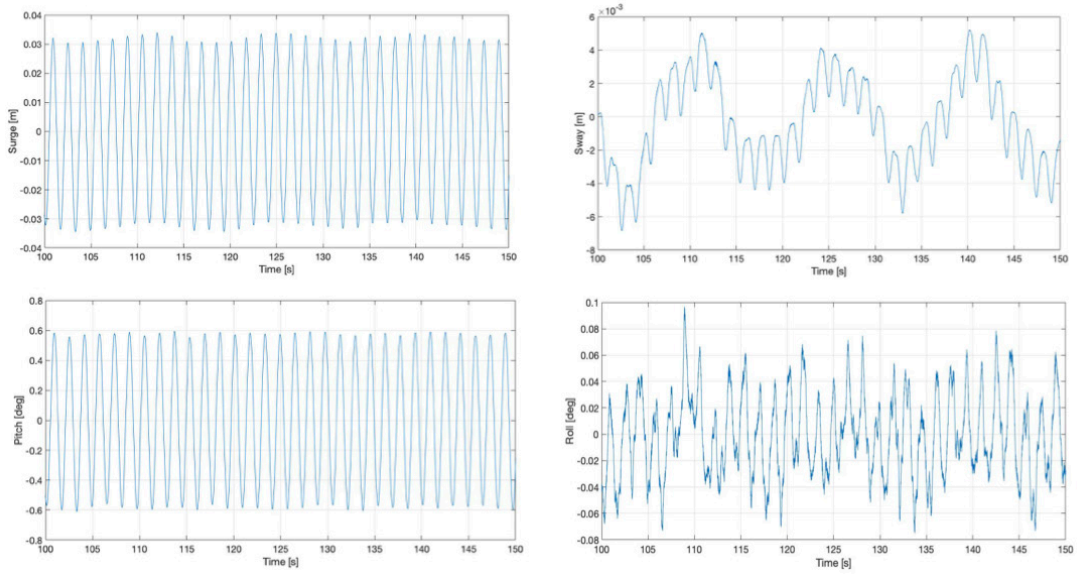


*Fig.5 - Sample time histories of surge, sway, roll and pitch measured in test #250.*

*Time and frequency domain analysis results*

Only part of the data set is analyzed in this manuscript. In particular, six tests with regular waves, defined by $H$ and $T$, respectively the wave height and the wave period, were selected for time and frequency domain analysis. In Table 5, the selected tests are listed together with the first, second and third wave harmonic and the natural frequencies for each DoF obtained from analysis of the free decay tests. Three tests refer to "no wind conditions" and three tests refer to "above rated conditions". For all selected tests, wave incidence was orthogonal to the structure.

As an example, sample time histories of surge, sway, roll and pitch of test #250 are shown in Figure 5. It is noted that the small quantities associated with a longitudinal motion are almost sinusoidal and the dominant wave frequency can be clearly seen. However, the small quantities associated with lateral motion, show different behavior, mainly dominated by their respective natural frequency, with the dominant wave frequency superimposed on it.

These findings are consistent for all tests analyzed and are further confirmed by frequency domain analysis. As an example, in Figure 6 the PSD of surge measured during test #250 is shown. The dominant wave frequency of 0.63 Hz is clearly identified. In addition, the second and third harmonics

| | *H [m]* | *T [s]* | *DIR [deg]* | *Wind Sp [m/s]* | *fr 1X Wave [Hz]* | *fr 2X Wave [Hz]* | *fr 3X Wave [Hz]* | *fr surge [Hz]* | *fr sway [Hz]* | *fr heave [Hz]* | *fr pitch [Hz]* | *fr roll [Hz]* | *fr yaw [Hz]* |
|---|---|---|---|---|---|---|---|---|---|---|---|---|---|
| ***Test 182*** | 0.05 | 1.6 | 0 | 0 | 0.63 | 1.25 | 1.87 | 0.09 | 0.07 | 0.22 | 0.20 | 0.18 | 0.39 |
| ***Test 250*** | 0.13 | 1.6 | 0 | 0 | 0.63 | 1.25 | 1.87 | 0.09 | 0.07 | 0.22 | 0.20 | 0.18 | 0.39 |
| ***Test 232*** | 0.25 | 1.6 | 0 | 0 | 0.63 | 1.25 | 1.87 | 0.09 | 0.07 | 0.22 | 0.20 | 0.18 | 0.39 |
| ***Test 277*** | 0.05 | 1.6 | 0 | 1.85 | 0.63 | 1.25 | 1.87 | 0.09 | / | 0.22 | 0.18 | 0.17 | 0.30 |
| ***Test 288*** | 0.13 | 1.6 | 0 | 1.85 | 0.63 | 1.25 | 1.87 | 0.09 | / | 0.22 | 0.18 | 0.17 | 0.30 |
| ***Test 337*** | 0.25 | 1.6 | 0 | 1.85 | 0.63 | 1.25 | 1.87 | 0.09 | / | 0.22 | 0.18 | 0.17 | 0.30 |

*Tab. 5 - Regular wave tests considered for frequency domain analysis*

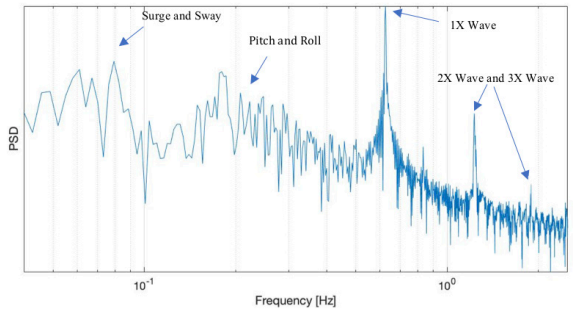


*Fig.6 - PSD of Surge as measured in test #250.*

are found at 1.25 Hz and 1.87 Hz, although for the considered case the contribution of the third harmonic is relatively low. The reason for this lies in the fact that the wave is closer to second order than to third order. So, the influence of this third harmonic is small. Finally, the natural frequencies of each DoF are pretty visible. These five frequencies are recognized in almost all measured signals, with different relative amplitudes, depending on wave height and wind condition.

The power spectrum of all selected tests was obtained for each parameter. Figures 7.1 through 7.4 show the PSDFs of surge, sway, pitch and roll as measured in tests 182-250-232 (no wind conditions) and 277-288-337 (above rated conditions), which have the same peak period and the same wind speed but different wave height.

To quantify the contribution of the different frequencies to the total response, Tables 6.1 through 6.3 show the power corresponding to narrow ranges around the relevant frequencies, together with the total power, STDs and peak factors to evaluate the expected maxima of the response parameters, knowing that some quantities of energy may be shared by more Dof with similar frequency.

In the tests for the longitudinal motions, the response is dominated by the fundamental wave frequency, while for lateral motions, a large amount of the excitation can be found at the respective natural frequencies.

For the longitudinal response, it is observed that the fundamental wave frequency contributes to the total surge from 54.9% to 99.6%, to the total pitch from 73.7% to 98.8% and to the total longitudinal acceleration form 98.3% to 99.9%.

Different behavior is noted in lateral response; for sway and roll the fundamental wave frequency is not always dominant, ranging from 7.2% to 71.6% to the total sway and from 15.8% to 52.0% to the total roll. Only in the case of lateral acceleration the fundamental wave frequency contributes in a dominant way from 98.4% to 99.9%.

Finally, the histograms of the occurrence frequencies of surge, sway, roll and pitch as evaluated from test #250 are shown in Figure 8. Consistently with what previously observed, it is

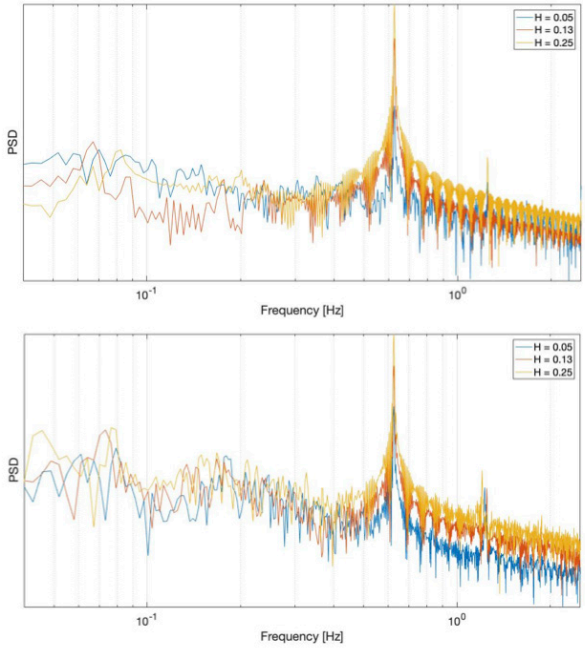


*Fig. 7.1- PSDFs of Surge as measured in no wind condition tests 182, 250, 232 (up) and above rated condition tests 277, 288, 337 (down).*

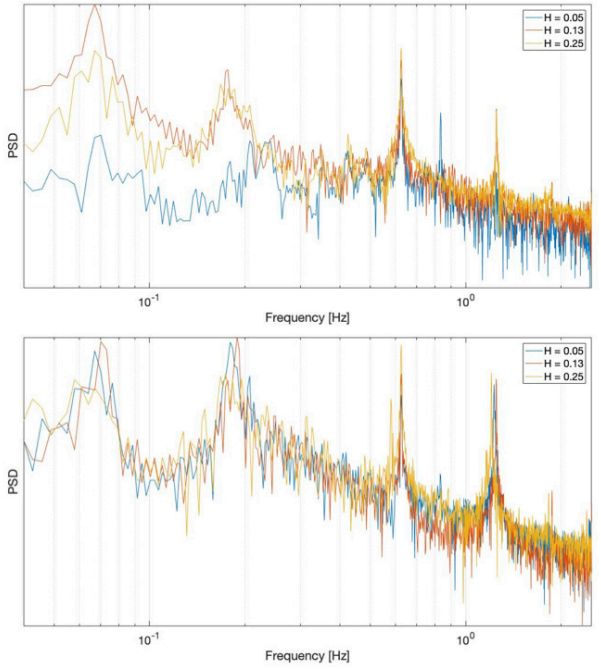


*Fig. 7.2- PSDFs of Sway as measured in no wind condition tests 182, 250, 232 (up) and above rated condition tests 277, 288, 337 (down).*

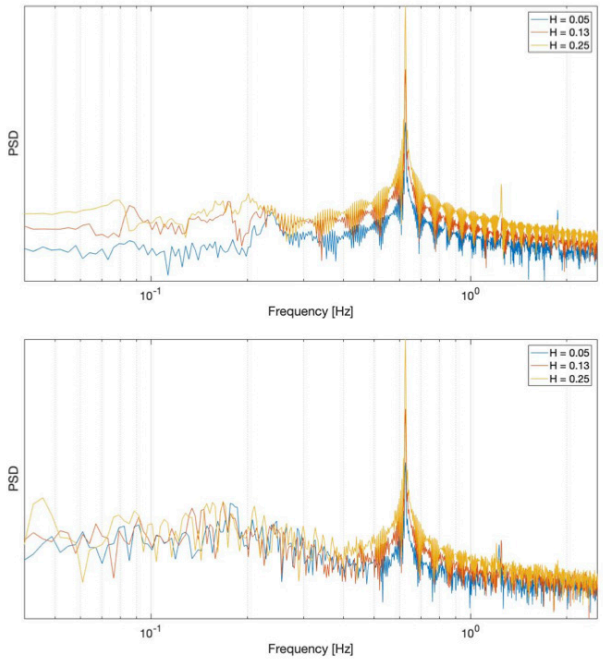


*Fig. 7.3- PSDFs of Pitch as measured in no wind condition tests 182, 250, 232 (up) and above rated condition tests 277, 288, 337 (down).*

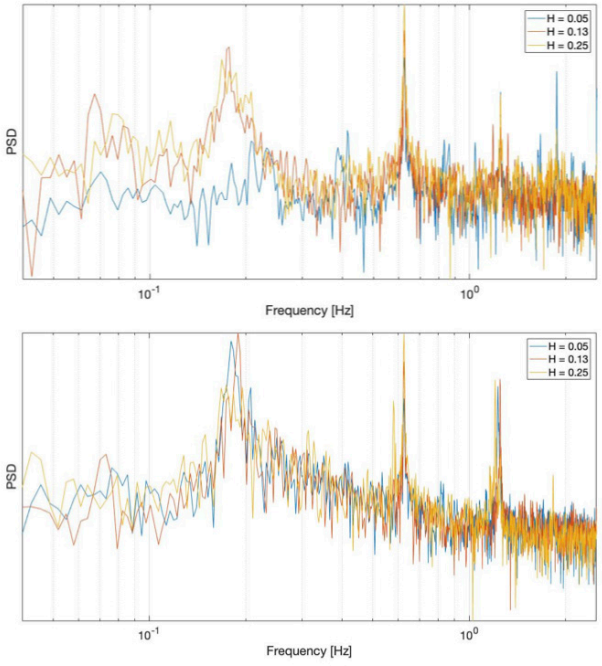


*Fig. 7.4- PSDFs of Roll as measured in no wind condition tests 182, 250, 232 (up) and above rated condition tests 277, 288, 337 (down).*

noticed that the quantities related to the longitudinal response feature a bimodal distribution, indicating an almost sinusoidal response. On the other hand, the histograms of the quantities related to the lateral response appear to be associated with the combination of the narrowband process and a broader band process, whose relative intensity depends on the particular quantity observed.

*Dynamic Forces*

With regard to the internal forces, in the same format, Table 7 shows the power corresponding to narrow ranges around the relevant frequencies for internal forces. The wave frequency is always dominant, with contributions ranging from 94.4% to 99.0% for the longitudinal forces, and from 32.0% to 82.5% for the lateral forces. Even in this case, the energy associated to the wave frequency in lateral response is lower than in longitudinal response, however the second harmonics are predominant. In support of this conclusions, Figure 9 shows the PSDF of lateral force at the nacelle.

*Mooring lines forces*

Analysis of the mooring line forces revealed a strong sensitivity of the measured data on the alignment of the lines with the oncoming waves. In the experimental setup, the mooring lines 2 and 3 are symmetric at an angle of 120° with mooring line 1 which was aligned with the oncoming waves behind the model. In Figure 10, a sample time history of the forces measured in test #250 at mooring lines 1 and 2 are shown, demonstrating that the dynamic force in the mooring line 2 located ahead of the model is larger than the dynamic force in the mooring lines 1 located behind the model.

In time histories it can be seen that the force in the mooring line 2 is dominated by first wave frequency and surge and sway frequencies while the force in mooring line 1 the greatest contribute comes from dominant wave frequency. In confirmation of this, in Figures 11.1 and 11.2, the PSDFs of the mooring lines tension for the conditions of “no wind” and “above rated” are shown. As displacement and acceleration spectra, the surge, sway, pitch and roll oscillations frequencies are clearly visible, together with the oncoming wave frequency and first, second and third harmonics. Table 8 shows the power corresponding to narrow ranges around the relevant frequencies, together with the total power of the force in mooring line 1 and 2, respectively. In this case, most of energy is concentrated at the wave frequency up to 97.0% of the total power, but not always it is the dominant one. In some tests, most of energy is concentrated at sway and surge frequency up to 58.5%.

Also in this case the dynamic forces are proportional to the oncoming wave height, whereas the mean forces are very little affected by it.

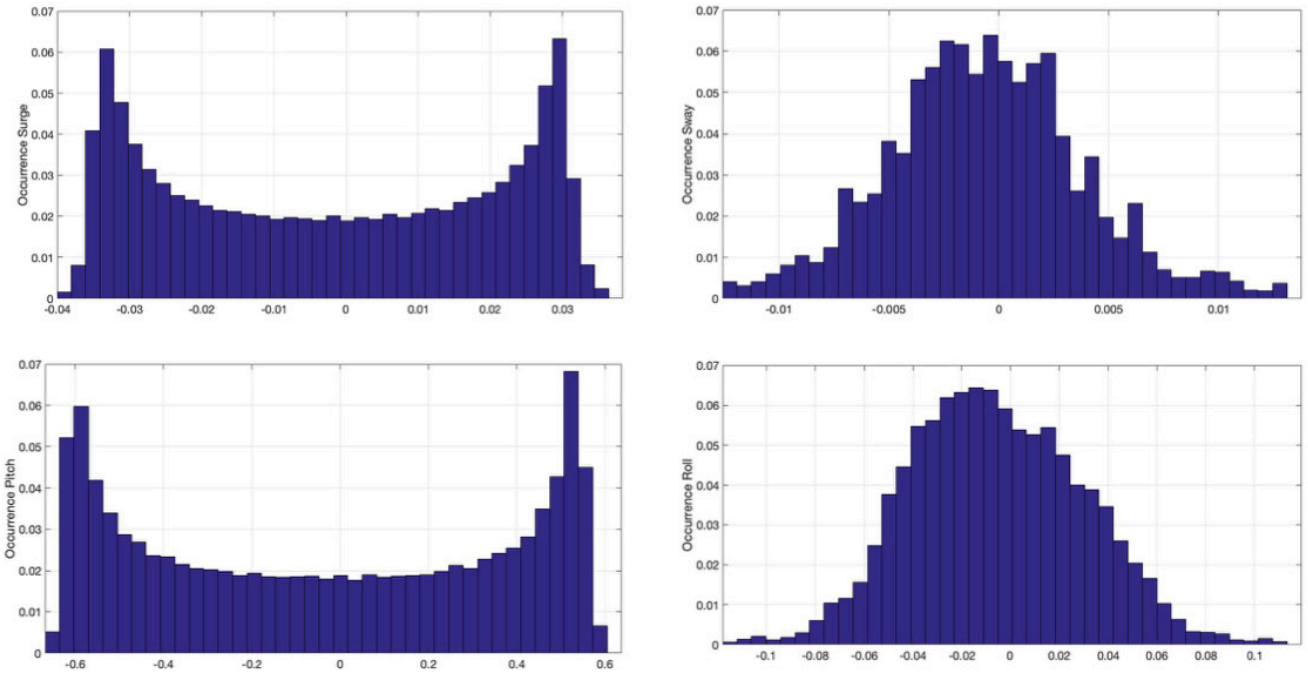


*Fig. 8 - Histograms of the occurrence frequencies of surge, sway, pitch and roll as measured in test #250.*

| | Surge narrow-band and total power | | | | | | Sway narrow-band and total power | | | | | |
|---|---|---|---|---|---|---|---|---|---|---|---|---|
| **Wind Condition** | **No Wind** | | | **Rated Condition** | | | **No Wind** | | | **Rated Condition** | | |
| **H [m]** | **0.05** | **0.13** | **0.25** | **0.05** | **0.13** | **0.25** | **0.05** | **0.13** | **0.25** | **0.05** | **0.13** | **0.25** |
| **1X Wave Frequency** | 54.9% | 99.6% | 90.9% | 71.2% | 89.4% | 95.4% | 71.6% | 20.7% | 34.9% | 8.4% | 7.2% | 36.4% |
| **2X Wave Frequency** | 8.3% | 0.3% | 7.2% | 2.6% | 2.8% | 0.0% | 0.1% | 1.4% | 7.2% | 10.3% | 6.0% | 13.1% |
| **3X Wave Frequency** | 0.2% | 0.0% | 0.1% | 0.2% | 0.1% | 0.0% | 0.0% | 0.5% | 0.0% | 0.1% | 0.2% | 2.3% |
| **Surge Frequency** | 11.1% | 0.2% | 0.4% | 2.3% | 4.7% | 1.1% | 1.7% | 15.6% | 18.9% | 2.7% | 4.4% | 5.0% |
| **Sway Frequency** | 10.8% | 0.3% | 0.3% | / | / | / | 3.6% | 39.3% | 30.1% | / | / | / |
| **Heave Frequency** | 0.2% | 0.0% | 0.0% | 3.8% | 0.2% | 0.3% | 2.8% | 5.1% | 10.5% | 7.2% | 2.7% | 3.4% |
| **Pitch Frequency** | 0.2% | 0.0% | 0.0% | 4.7% | 1.2% | 0.2% | 2.8% | 16.1% | 11.5% | 30.1% | 27.9% | 8.7% |
| **Roll Frequency** | 0.5% | 0.0% | 0.0% | 5.1% | 2.2% | 0.3% | 1.0% | 23.0% | 21.2% | 34.1% | 31.9% | 11.7% |
| **Yaw Frequency** | 0.3% | 0.0% | 0.0% | 1.5% | 0.6% | 0.1% | 0.1% | 0.0% | 5.0% | 5.7% | 6.5% | 4.2% |
| **STD** | 0.00 | 0.02 | 0.04 | 0.01 | 0.02 | 0.00 | 0.00 | 0.00 | 0.00 | 0.01 | 0.01 | 0.00 |
| **Peak Factor** | 1.01 | 1.03 | 1.05 | 1.03 | 1.05 | 0.00 | 1.02 | 1.16 | 1.07 | 1.36 | 1.32 | 0.00 |

*Tab. 6.1 -Surge and Sway narrow-band and total power.*

| | Pitch narrow-band and total power | | | | | | Roll narrow-band and total power | | | | | |
|---|---|---|---|---|---|---|---|---|---|---|---|---|
| **Wind Condition** | **No Wind** | | | **Rated Condition** | | | **No Wind** | | | **Rated Condition** | | |
| **H [m]** | **0.05** | **0.13** | **0.25** | **0.05** | **0.13** | **0.25** | **0.05** | **0.13** | **0.25** | **0.05** | **0.13** | **0.25** |
| **1X Wave Frequency** | 96.9% | 98.8% | 97.9% | 73.7% | 92.3% | 96.4% | 46.0% | 43.9% | 52.0% | 15.8% | 25.2% | 47.4% |
| **2X Wave Frequency** | 0.3% | 0.0% | 0.5% | 0.3% | 0.5% | 0.1% | 21.6% | 6.0% | 14.1% | 18.3% | 11.0% | 9.7% |
| **3X Wave Frequency** | 1.3% | 0.0% | 0.0% | 0.0% | 0.0% | 0.0% | 25.4% | 2.2% | 3.0% | 0.1% | 0.0% | 2.0% |
| **Surge Frequency** | 0.0% | 0.2% | 0.1% | 2.1% | 0.6% | 0.4% | 0.4% | 4.9% | 1.2% | 0.6% | 0.7% | 0.2% |
| **Sway Frequency** | 0.0% | 0.1% | 0.3% | / | / | / | 0.5% | 5.4% | 1.3% | / | / | / |
| **Heave Frequency** | 0.0% | 0.3% | 0.2% | 1.7% | 0.3% | 0.5% | 3.3% | 1.0% | 0.9% | 8.9% | 6.2% | 6.7% |
| **Pitch Frequency** | 0.0% | 0.1% | 0.2% | 6.3% | 2.3% | 0.6% | 3.3% | 7.0% | 18.9% | 29.9% | 29.1% | 12.0% |
| **Roll Frequency** | 0.0% | 0.2% | 0.1% | 9.3% | 2.5% | 0.8% | 1.6% | 38.8% | 23.6% | 31.5% | 35.9% | 15.6% |
| **Yaw Frequency** | 0.0% | 0.0% | 0.0% | 3.4% | 0.8% | 0.2% | 1.9% | 0.0% | 0.2% | 8.7% | 7.8% | 6.2% |
| **STD** | 0.13 | 0.40 | 0.77 | 0.19 | 0.43 | 0.81 | 0.03 | 0.04 | 0.05 | 0.22 | 0.22 | 0.22 |
| **Peak Factor** | 1.16 | 1.43 | 1.66 | 1.08 | 1.13 | 1.29 | 1.10 | 1.14 | 1.12 | 1.57 | 1.41 | 1.60 |

*Tab. 6.2 -Pitch and Roll narrow-band and total power.*

| | Acceleration ax,base narrow-band and total power | | | | | | Acceleration ay,top narrow-band and total power | | | | | |
|---|---|---|---|---|---|---|---|---|---|---|---|---|
| **Wind Condition** | **No Wind** | | | **Rated Condition** | | | **No Wind** | | | **Rated Condition** | | |
| **H [m]** | **0.05** | **0.13** | **0.25** | **0.05** | **0.13** | **0.25** | **0.05** | **0.13** | **0.25** | **0.05** | **0.13** | **0.25** |
| **1X Wave Frequency** | 98.3% | 99.7% | 99.9% | 98.3% | 99.4% | 99.7% | 98.4% | 99.7% | 99.9% | 98.5% | 99.6% | 99.7% |
| **2X Wave Frequency** | 0.1% | 0.1% | 0.2% | 2.4% | 0.2% | 0.1% | 0.0% | 0.3% | 0.0% | 1.1% | 9.4% | 0.3% |
| **3X Wave Frequency** | 0.0% | 0.0% | 0.0% | 0.0% | 0.1% | 0.1% | 0.1% | 0.0% | 0.2% | 0.1% | 0.1% | 0.2% |
| **Surge Frequency** | 0.1% | 0.0% | 0.0% | 0.1% | 0.0% | 0.0% | 0.0% | 0.0% | 0.0% | 0.1% | 0.0% | 0.0% |
| **Sway Frequency** | 0.1% | 0.0% | 0.0% | / | / | / | 0.1% | 0.0% | 0.0% | / | / | / |
| **Heave Frequency** | 0.1% | 0.0% | 0.0% | 0.3% | 0.1% | 0.1% | 0.0% | 0.0% | 0.0% | 0.2% | 0.0% | 0.1% |
| **Pitch Frequency** | 0.1% | 0.0% | 0.0% | 0.3% | 0.1% | 0.0% | 0.0% | 0.0% | 0.0% | 0.3% | 0.1% | 0.0% |
| **Roll Frequency** | 0.0% | 0.0% | 0.0% | 0.3% | 0.1% | 0.0% | 0.0% | 0.0% | 0.0% | 0.3% | 0.1% | 0.0% |
| **Yaw Frequency** | 0.1% | 0.0% | 0.0% | 0.3% | 0.1% | 0.0% | 0.1% | 0.0% | 0.0% | 0.4% | 0.0% | 0.0% |
| **STD** | 0.02 | 0.06 | 0.11 | 0.03 | 0.06 | 0.11 | 0.03 | 0.07 | 0.13 | 0.04 | 0.08 | 0.15 |
| **Peak Factor** | 1.01 | 1.01 | 1.02 | 1.01 | 1.01 | 1.02 | 1.01 | 1.01 | 1.02 | 1.01 | 1.02 | 1.03 |

*Tab. 6.3 -Acceleration ax,base and ay,top narrow-band and total power.*

| | Force Fx,nacelle narrow-band and total power | | | | | | Force Fy,nacelle narrow-band and total power | | | | | |
|---|---|---|---|---|---|---|---|---|---|---|---|---|
| **Wind Condition** | **No Wind** | | | **Rated Condition** | | | **No Wind** | | | **Rated Condition** | | |
| **H [m]** | **0.05** | **0.13** | **0.25** | **0.05** | **0.13** | **0.25** | **0.05** | **0.13** | **0.25** | **0.05** | **0.13** | **0.25** |
| **1X Wave Frequency** | 98.1% | 99.0% | 98.6% | 97.3% | 94.4% | 95.6% | 82.5% | 76.3% | 77.1% | 32.0% | 28.0% | 35.6% |
| **2X Wave Frequency** | 0.6% | 0.4% | 1.1% | 1.6% | 4.7% | 3.2% | 12.2% | 9.0% | 12.0% | 42.6% | 30.1% | 37.9% |
| **3X Wave Frequency** | 0.2% | 0.3% | 0.3% | 0.1% | 0.0% | 0.3% | 0.2% | 5.1% | 5.3% | 7.6% | 4.5% | 15.7% |
| **Surge Frequency** | 0.2% | 0.1% | 0.4% | 0.3% | 0.1% | 0.0% | 0.1% | 0.0% | 0.0% | 0.3% | 0.8% | 0.3% |
| **Sway Frequency** | 0.3% | 0.0% | 0.0% | / | / | / | 0.0% | 0.2% | 0.1% | / | / | / |
| **Heave Frequency** | 0.0% | 0.0% | 0.0% | 0.1% | 0.0% | 0.2% | 1.1% | 0.0% | 0.0% | 6.4% | 1.9% | 2.9% |
| **Pitch Frequency** | 0.1% | 0.1% | 0.2% | 0.3% | 0.1% | 0.2% | 0.8% | 6.6% | 5.0% | 20.5% | 16.6% | 12.1% |
| **Roll Frequency** | 0.2% | 0.0% | 0.1% | 0.3% | 0.1% | 0.0% | 0.2% | 7.9% | 7.1% | 24.9% | 20.7% | 13.1% |
| **Yaw Frequency** | 0.0% | 0.0% | 0.0% | 0.2% | 0.0% | 0.0% | 0.0% | 0.0% | 0.0% | 14.0% | 9.2% | 5.2% |
| **STD** | 1.54 | 3.99 | 7.67 | 2.11 | 4.50 | 8.14 | 0.16 | 0.35 | 0.57 | 2.71 | 3.07 | 2.22 |
| **Peak Factor** | 1.90 | 1.72 | 1.91 | 1.27 | 1.38 | 1.70 | 1.15 | 1.24 | 1.59 | 2.16 | 2.08 | 2.22 |

*Tab. 7 - Forces Fx,nacelle and Fy,nacelle narrow-band and total power*

| | Mooring line 1 narrow-band and total power | | | | | | Mooring line 2 narrow-band and total power | | | | | |
|---|---|---|---|---|---|---|---|---|---|---|---|---|
| **Wind Condition** | **No Wind** | | | **Rated Condition** | | | **No Wind** | | | **Rated Condition** | | |
| **H [m]** | **0.05** | **0.13** | **0.25** | **0.05** | **0.13** | **0.25** | **0.05** | **0.13** | **0.25** | **0.05** | **0.13** | **0.25** |
| **1X Wave Frequency** | 97.0% | 95.3% | 92.1% | 32.9% | 45.0% | 67.7% | 96.1% | 57.8% | 85.4% | 25.9% | 30.0% | 57.4% |
| **2X Wave Frequency** | 0.2% | 0.0% | 2.8% | 0.0% | 0.5% | 4.6% | 0.0% | 0.1% | 7.1% | 0.1% | 0.8% | 6.8% |
| **3X Wave Frequency** | 0.0% | 0.0% | 0.6% | 0.1% | 0.0% | 0.3% | 0.0% | 0.0% | 2.4% | 0.0% | 0.1% | 0.1% |
| **Surge Frequency** | 0.1% | 1.4% | 0.7% | 26.8% | 23.9% | 7.9% | 0.5% | 17.6% | 1.3% | 11.2% | 28.3% | 16.0% |
| **Sway Frequency** | 0.1% | 4.2% | 5.9% | 24.2% | 38.2% | 12.4% | 0.6% | 45.9% | 5.1% | 58.5% | 40.5% | 23.8% |
| **Heave Frequency** | 0.1% | 0.0% | 0.2% | 0.6% | 0.4% | 0.2% | 0.1% | 0.0% | 0.2% | 0.6% | 0.7% | 3.1% |
| **Pitch Frequency** | 0.0% | 0.0% | 0.0% | 0.8% | 0.3% | 0.0% | 0.1% | 0.1% | 0.3% | 0.4% | 0.2% | 0.6% |
| **Roll Frequency** | 0.0% | 0.1% | 0.0% | 0.8% | 0.3% | 0.1% | 0.0% | 0.2% | 0.3% | 0.2% | 0.0% | 0.0% |
| **Yaw Frequency** | 0.0% | 0.0% | 0.0% | 1.0% | 0.1% | 0.0% | 0.0% | 0.0% | 0.0% | 0.1% | 0.0% | 0.1% |
| **STD** | 0.01 | 0.02 | 0.03 | 0.01 | 0.03 | 0.05 | 0.00 | 0.02 | 0.02 | 0.01 | 0.02 | 0.02 |
| **Peak Factor** | 1.01 | 1.03 | 1.05 | 1.05 | 1.08 | 1.12 | 1.01 | 1.03 | 1.03 | 1.02 | 1.03 | 1.03 |

*Tab. 8 - Mooring line 1 and Mooring line 2 forces narrowband and total power.*

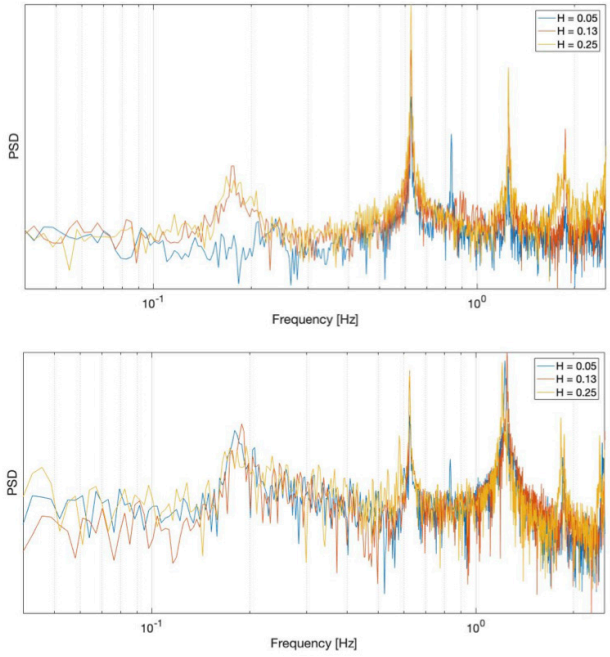


*Fig. 9 - PSDFs of the force in y-direction at nacelle as measured in no wind condition tests 182, 250, 232 (up) and above rated condition tests 277, 288, 337 (down).*

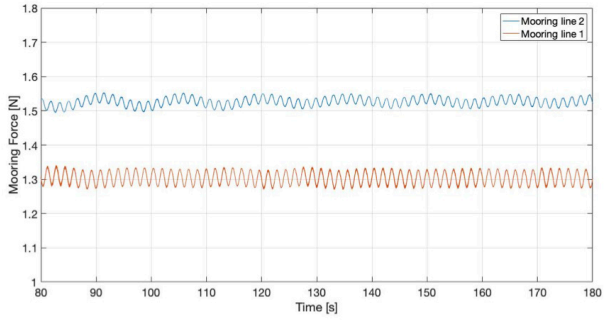


*Fig. 10 - Sample time histories of mooring line forces for test #250.*

## CONCLUSIONS

In the present paper, the behavior of a model-scaled Spar Buoy Wind Turbine has been observed in order to investigate the dynamic behavior for different wave and wind conditions.

Regular waves with a given wave period and different wave heights have been considered, in absence of wind load and with a value of wind speed that lead the above rated condition of the wind turbine rotor. Displacements, accelerations, tower forces and mooring line forces have been measured and analysed.

Free decay tests were carried out to detect the natural periods of each DoF and the damping ratios; natural frequencies of order of ($10^{-2}$) were found for the surge and sway motions and of order of ($10^{-1}$) for the roll and pitch motions.

The damping coming from free decay test were also calculated. Besides reaching the coefficient representing the exponentially decaying sinusoid, damping ratios of 14.7%, 11.1%, 4.3%, 3.4%, 6.0%, 3.3% and 8.5% were found from free

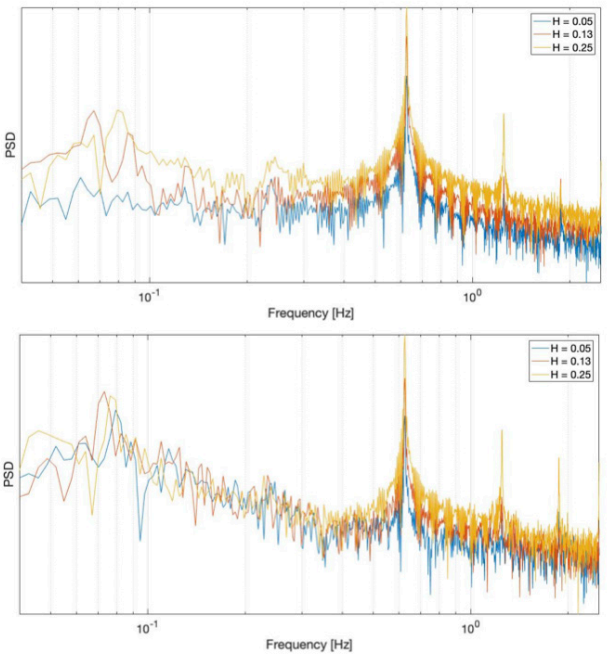


*Fig. 11.1 -PSDFs of Mooring line1 as measured in no wind condition tests 182, 250, 232 (up) and above rated condition tests 277, 288, 337 (down).*

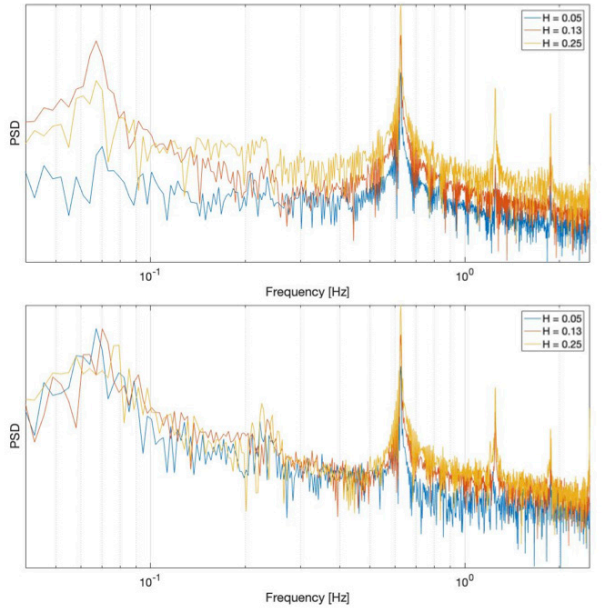


*Fig. 11.2 -PSDFs of Mooring line2 as measured in no wind condition tests 182, 250, 232 (up) and above rated condition tests 277, 288, 337 (down).*

decay oscillations for surge, sway, roll and pitch, respectively when the first 7 cycles of oscillation were considered.

Analysis of the dynamic response have been carried out in terms of displacements, accelerations and tower and mooring line forces. It reveals that for the displacements and rotations associated with the longitudinal response, the behavior is dominated by the wave frequency, but for the same parameters associated with the lateral response, the wave frequency is not always dominant and most of energy lies within its DoF.

It is noticed that at higher frequencies the response increases with wave height both without and with the wind load; this trend is most prominent in presence of wind, suggesting that the gyroscopic effects and the rotor dynamics can partially affect the dynamic response.

## ACKNOWLEDGEMENTS

The coordinator, Roberto Tomasicchio, thanks Mark Klein Breteler from Deltares and Bjarne Jensen from Danish Hydraulics Institute for their advices and patience since the submission of the proposal. The Users Group thanks DHI for the warm hospitality and the technicians for their assistance. This project has received funding from the European Union's Horizon 2020 research and innovation programme under grant agreement No 654110, HYDRALAB+.

## REFERENCES

Booij N., Ris R.C. & Holthuijsen LH (1999) - *A third-generation wave model for coastal regions. 1. Model Description and validation* - J. Geophys. Res, **104**: 7649 - 7666.

Wind Europe (2019) - *Offshore Wind in Europe. Key trends and statistics 2018.* Retrieved March 28, 2019, from https://windeurope.org/about-wind/statistics/european/wind-energy-in-europe-in-2018/.

Bilgili M., Yasar A. & Simsek E. (2011) - *Offshore wind power development in Europe and its comparison with onshore counterpart.* Renewable and Sustainable Energy Reviews, **15** (2).

Breton S. & Moe G. (2009) - *Status, plans and technologies for offshore wind turbines in Europe and North America.* Renewable Energy, **34** (3): 646 - 654.

Groupee A.J., Koo B.J., Kimball R.W., Lambrakos K.F. & Dagher H.J. - *Experimental comparison of three floating wind turbine concepts.* Journal of Offshore Mechanics and Arctic Engineering, **136** (2): 020906.

Jonkman J. (2010) - *Definition of the Floating System for Phase IV of OC3 (No. NREL/TP-500-47535)*. National Renewable Energy Lab (NREL). Golden, CO, USA.

Jonkman J., Larsen T., Hansen A., Nygaard T., Maus K., Karimirad M. & Fylling I. (2010 - *Offshore code comparison collaboration within IEA Wind Task 23: Phase IV results regarding floating wind turbine modeling*. National Renewable Energy Lab. (NREL), Golden, CO (United States).

Karimirad M. (2014) - *Offshore Energy Structures For Wind Power, Wave Energy and Hybrid Marine Platforms Coastal.* Springer.

Mansard E.P.D. & Funke E.R. (1980) - *The measurement of incident and reflected spectra using a least squares method.* Coastal Engineering, 154 - 172.

Petaccia G., Persi e., Sibilla s., Brufau, p., & García-navarro P. (2018) - *Enhanced one-way coupled swe-de model for floating body transport*. Italian Journal Eng. Geol. Environ., **1**.

Riefolo L., Del Jesus F., Guanche R. G., Tomasicchio G. R. & Pantusa D. (2018). - *Wind/wave misalignment effects on mooring line tensions for a spar buoy wind turbine.* Proceedings of the International Conference on Ocean, Offshore and Arctic Engineering (OMAE2018), Madrid, Spain, June 17 - 22, paper n° omae2018-77586.

Riefolo L., Lanfredi C., Azzellino A., Vicinanza D., Tomasicchio G. R., D'Alessandro F. & Penchev V. (2016). - *Offshore wind turbines: an overview of the effects on the marine environment*. Proceedings of the twenty-sixth International Society of Offshore and Polar Engineering Conference (ISOPE), Rhodes, greece, 26 june - 2 july, 427 - 434.

Roald L., Jonkman J., Robertson A. & Chokani N. (2013). *The effect of second-order hydrodynamics on floating offshore wind turbines.* Energy Procedia, **35**: 253 - 264.

Stockstill R. L., Daly D. F. & Hopkins M.A. (2009) - *Modeling floating objects at river structures.* Journal. Hydraul., **135** (5): 403 - 414. http://dx.doi:10.1061/(asce)0733-9429(2009)135:5(403).

Sumer Mutlu M., (2006) - *Hydrodynamics around cylindrical structures.* Vol. **26**. World scientific.

Tomasicchio G. R., Avossa A. M., Riefolo L., Ricciardelli F., Musci E., D'Alessandro F. & Vicinanza D. (2016) - *Dynamic Modelling Of A Spar Buoy Wind Turbine.* 36th International Conference on Ocean, Offshore and Arctic Engineering (OMAE 2017) June 25 - 30, Trondheim, Norway, Paper N. OMAE2017-62246, pg. V010T09A083-V010T09A093; doi:10.1115/OMAE2017-62246.

Tomasicchio G.R., D'alessandro F., Avossa A.M., Riefolo L., Musci E., Ricciardelli F. & Vicinanza D. (2018) - *Experimental modelling of the dynamic behaviour of a spar buoy wind turbine.* Renewable energy, **127**: 412 - 432.

Tomasicchio G. R., Armenio E., D'Alessandro F., Fonseca N., Mavrakos S. A., Penchev V., Schüttrumpf H. & Voutsinas S. (2012) - *Design of a 3d physical and numerical experiment on floating off-shore wind turbines*. Proc. 33th International Conf. on Coastal Engineering, Santander, n. **67**.

*Received September 2019 - Accepted January 2020*